Mechanism of Thermally Induced Morphological Reorganization and Lamellar Orientation from the Herringbone Structure in Cross-Linked Polystyrene-*block*-polybutadiene-*block*-polystyrene Triblock Copolymers

Shinichi Sakurai,*,† Sakae Aida,† Shigeru Okamoto,‡ Kazuo Sakurai,§ and Shunji Nomura†

Department of Polymer Science & Engineering, Kyoto Institute of Technology, Matsugasaki, Sakyo-ku, Kyoto 606-8585, Japan; Department of Material Science and Engineering, Nagoya Institute of Technology, Gokiso-cho, Showa-ku, Nagoya 466-8555, Japan; and Department of Chemical Processes and Environments, The University of Kitakyushu, 1-1, Hibikino, Wakamatsu-ku, Kitakyushu, 808-0135 Japan

Received December 28, 2001

ABSTRACT: Structural transformation from the herringbone structure to the preferentially oriented lamellae under the elongational flow has been studied by the two-dimensional small-angle X-ray scattering (2d-SAXS) technique. For this purpose, thermoplastic elastomer SBS (polystyrene-*block*-polybutadiene-*block*-polystyrene) triblock copolymer samples were used. The lamellar samples of which polybutadiene chains were chemically cross-linked in advance are subjected to be fractured by a uniaxial stretching at room temperature. Thus, the herringbone structure resulted. Then, the samples were further subjected to the elongational flow at an elevated temperature above the glass transition temperature of polystyrene. The process of the structural transformation was followed by the time-resolved 2d-SAXS measurement using synchrotron radiation upon temperature jump (T-jump) from room temperature for the uniaxially stretched SBS sample. A characteristic *parallel streak pattern* of 2d-SAXS was observed for the herringbone structure, which transformed rapidly into an *oblique streak pattern* upon the T-jump, gradually emerging into a *two-spot pattern* as time went on. Various structural parameters can be evaluated to characterize truncated lamellae and grains (size and orientation). On the basis of the results characterizing the transient structures, the mechanism of the structural transformation was considered. It was found that the process is different depending on the degree of cross-linking. However, commonly the process was found to be divided into three regions (I, II, and III). These regions are governed by the balance between *perpendicular orientation* of the truncated lamellae within the grain and *parallel orientation* of the PS lamellae with respect to the stretching direction. The corresponding orientational relaxation of the PB chains was also examined by the time-resolved Fourier transformed infrared spectroscopic measurements. The conformational changes of the PB chain were found to play a role in controlling the lamellar repeat distance in regions I and II, to which respectively further chain stretching and orientational relaxation of the PB chain were relevant.

I. Introduction

Block copolymers undergo microphase separation transition and spontaneously form regularly ordered microdomain structure. The morphology of the microdomain structure is rich in variety, such as spheres, cylinders, gyroid, and lamellae.[1] It is well-known that the morphology can be controlled by the composition of the block copolymers.[2−6] The difference in the chain dimensions between A and B block chains determines the curvature of an interface and hence the three-dimensional shape of the microdomains. Not only the shape of microdomains but their spatial arrangement are controlled by the interplay of chain conformations of A and B blocks. As a result, spatial symmetry is spontaneously generated, such as bcc (body-centered cubic), hexagonal, $Ia\bar{3}d$, or a one-dimensionally alternating superlattice on a nanometer scale for the above-mentioned morphologies. Such spatial order sometimes extends over tens of microns.[7] Therefore, block copolymers are excellent models to visualize the statistical mechanical properties of chain molecules through a variety of morphologies.

Since the spatial order extends over microns, the microdomain structure affects macroscopic properties. In this regard, defects in the structure impair precise control of the properties. Therefore, a defect-free single crystal of the microdomain is desired just as in single-crystal organic or inorganic materials, and defect annihilation dynamics and the growth mechanism of a grain are worthy of study. Many studies utilizing various kinds of the external fields have been conducted to align microdomains and in turn to reduce the number of defects.[8−25] For this kind of study, the block copolymer consisting of glassy and rubbery microdomains provides a good example. The glassy microdomains undergo fracture when the block copolymer sample is mechanically deformed.[26] Typically for glassy lamellae, it has been found that the herringbone structure (refer to Figure 6b) results from the fracture,[26−28] and the spontaneous healing of the fractured lamellar structure has been also known.[26] Since an external field such as elongational flow is effective in aligning cylindrical or lamellar microdomains,[22,24] healing in the flow field may result in the structural transformation from the herringbone structure toward well-aligned lamellae. The process is expected to be rich in variety due to the

† Kyoto Institute of Technology.
‡ Nagoya Institute of Technology.
§ The University of Kitakyushu.
* To whom all correspondence should be addressed: e-mail shin@ipc.kit.ac.jp.

10.1021/ma012259n CCC: $25.00
Published on Web 02/28/2003

dynamic interplay between flow-induced domain orientation, spontaneous domain orientation within a grain, and growth of grains. Although it has been revealed that the healing of the fractured glassy lamellae takes place above the glass transition temperature (T_g) of the glassy component,[26] the flow-induced ordering of the fractured lamellae from the herringbone structure has not yet been intensively studied due to experimental difficulties. Since we have found that chemical cross-links are instrumental in the flow orientation of lamellar microdomains above T_g of polystyrene ($T_{g,PS}$) in our previous studies using thermoplastic elastomer SBS (polystyrene-*block*-polybutadiene-*block*-polystyrene) triblock copolymer samples,[22,25] we closely examine in the current study the mechanism of the structural transformation from the herringbone structure toward the preferentially oriented lamellae under the elongational flow.

The two-dimensional small-angle X-ray scattering (2d-SAXS) technique was employed for the structural analyses. In this paper, the experimental (2d-SAXS) results are summarized in the Results section, and then the mechanism of the structural transformation from the herringbone structure is discussed in the Discussion section in relation to conformational changes of the polybutadiene (PB) block chains.

II. Experimental Section

II.A. Sample Preparation. The SBS triblock copolymer used in this study has the following molecular characteristics: $M_n = 6.31 \times 10^4$, $M_w/M_n = 1.15$, and $\phi_{PS} = 0.56$ where M_n and M_w denote the number-average and weight-average molecular weights, respectively, and ϕ_{PS} is the volume fraction of the PS blocks. The SBS sample and the cross-linker, which is (1,1-bis(*tert*-butylperoxy)-3,3,5-trimethylcyclohexane) to cross-link the PB chains, were dissolved in toluene (the polymer concentration was ca. 5 wt %). Then, the solution was poured into a flat Petri dish to allow gradual evaporation of the solvent. After complete evaporation for ca. 7 days at room temperature, an as-cast film was obtained with ca. 0.1 mm thickness. To activate the cross-linker, the as-cast sample was annealed thermally at 150 °C for 100 min.

For the qualitative characterization of the cross-linked material, we evaluated the weight fraction of the macroscopically cross-linked SBS molecules, $f_{network}$ (wt %), which is defined by $f_{network} = w_{network}/w_0 \times 100$, with $w_{network}$ and w_0 being respectively the weight of the macroscopically cross-linked SBS molecules and that of an as-cross-linked material containing un-cross-linked SBS components. To experimentally evaluate $w_{network}$, the as-cross-linked material was subjected to a rinse in toluene for 20 days so as to extract the un-cross-linked components. For this purpose, the toluene was refreshed every 2 days. In Figure 1, the $f_{network}$ shows a nonlinear dependency with the concentration of the cross-linker (c_X). For $c_X = 0.2$ wt %, $f_{network}$ almost reaches 80 wt %, and $f_{network} = 98$ wt % for $c_X = 1.5$ wt %. Note that the results obtained for $c_X = 0.5$ and 1.5 wt % are compared in this study as lightly ($f_{network} = 86$ wt %) and heavily ($f_{network} = 98$ wt %) cross-linked extremes, respectively.

We conducted uniaxial stretching at room temperature for the SBS samples of which PB lamellae were cross-linked chemically by the cross-linker. The final stretching ratio ϵ ($\epsilon = l/l_0$, where l and l_0 denote lengths of the film at stretched and unstretched state, respectively) for the uniaxial drawing is $\epsilon = 3.0$. Figure 2 displays changes in nominal stress during sample preparation. The full and broken lines show results for samples cross-linked with $c_X = 0.5$ and 1.5 wt %, respectively. The film sample was first uniaxially stretched up to $\epsilon = 3$ with the strain rate of 0.056 s^{-1} at room temperature. Both of the samples exhibit abrupt increase in stress with macroscopic necking in the initial stage of the stretching. Then, the stress decreased a bit and remained constant up to $\epsilon = 3.0$.

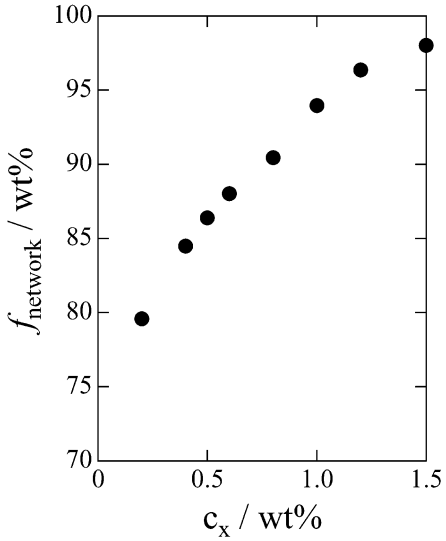

Figure 1. Plot of the weight fraction of the macroscopically cross-linked SBS molecules, $f_{network}$ (wt %), as a function of the concentration of cross-linker (c_X). The $f_{network}$ is defined by $f_{network} = w_{network}/w_0 \times 100$ with $w_{network}$ and w_0 being respectively weights of the macroscopically cross-linked SBS molecules and the as-cross-linked material containing un-cross-linked SBS components.

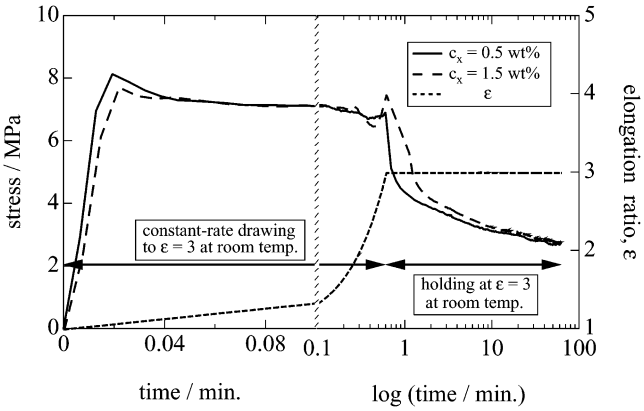

Figure 2. Changes in tensile stress during the sample preparation at room temperature for cross-linked SBS samples with concentrations of the cross-linker 0.5 and 1.5 wt %. The samples were stretched up to the elongation ratio $\epsilon = 3$, and then they were left attached in the stretching device for 60 min under stretched state at $\epsilon = 3$.

No further stretching of the sample was performed above $\epsilon = 3$. The stress relaxation was observed in the successive stage, where the sample was left attached in the stretching device, with its extent of ca. 55% decrease, irrespective of the degree of cross-linking. It was found that the stress relaxation was almost completed within about 50 min. On the basis of this result, we decided to leave samples stretched in the device for 60 min to equilibrate the stress for the further experiments of structural transformation at an elevated temperature above $T_{g,PS}$.

II.B. Two-Dimensional SAXS Measurements (2d-SAXS). The two-dimensional SAXS technique (2d-SAXS) is useful for the structural analysis of the herringbone structure and the transient structures in the course of transformation from the herringbone to oriented lamellae. To induce the structural transformation from the herringbone structure, after 60 min equilibration, the stretched sample with $\epsilon = 3.0$ was rapidly placed into the SAXS sample holder that was set in advance to 110 °C (above $T_{g,PS}$). Then the process was followed by the time-resolved 2d-SAXS measurement with the typical time slice of 10−30 s. The experiments were performed at the BL-15A (SAXS beamline) in the Photon Factory of the Research

Organization for High Energy Accelerator, Tsukuba, Japan. The Hamamatsu image intensifier with a cooled CCD[29] was used as a detector. No subtraction of the air scattering was conducted. The wavelength of X-rays, λ, was tuned at $\lambda = 0.1504$ nm.

II.C. Fourier Transform Infrared Spectroscopic Measurements (FTIR). The segmental orientations of PS and PB chains were examined by the Fourier transform infrared spectroscopic measurements. Infrared spectrograms were obtained using a Spectrum GX (Perkin-Elmer Japan Co., Ltd.) operating at a number of scans of 64 and a spectral resolution of 4 cm^{-1}. Rectangularly shaped films 30 mm long, 10 mm wide, and 0.1 mm thick were subjected to the measurements. The absorbance is given by $A = -\ln(I/I_0)$, where I and I_0 designate intensity of the transmitted infrared beam and incident beam, respectively. Since the observed FTIR spectrum comprises several individual absorption peaks overlapping each other, computational peak decomposition was performed to retrieve individual contributions. The numerical peak decomposition was performed, where the individual peak is assumed to be represented by a weighted sum of Gaussian and Lorentzian contributions. In the present study, we focus attention on the segmental orientation of PS and PB block chains. According to the method reported,[30,31] the values of the dichroic ratio orientation factor, F_D [$= (A_{\parallel} - A_{\perp})/(A_{\parallel} + 2A_{\perp})$], were obtained for PB from the dichroic ratio of the absorption band at 966 cm^{-1}, which is ascribed to an out-of-plane CH bending mode in *trans*-1,4-PB. Here, $A_{\parallel}$ and $A_{\perp}$ are the absorbances of the IR beam polarized parallel and perpendicular to the stretching direction, respectively. The values of F_D were also evaluated for PS using the absorption band at 1493 cm^{-1}, which is ascribed to a phenyl ring deformation mode in the direction parallel to the C−C bond between the main chain and phenyl ring.[30,31]

To reveal a temporal change in the chain stretching at 110 °C, which is the same temperature of the 2d-SAXS measurements, time-resolved FTIR measurements were conducted with the time slice of 10 s. Because of limitations of the instrument, it was impossible to synchronize switching of the polarizing angle of the IR beam between parallel and perpendicular to the stretching direction alternatingly with the series of the time slices of the FTIR measurements. Therefore, we separately conducted two individual runs of the time-resolved FTIR measurements with the IR beams parallel and perpendicular to the stretching direction, which give temporal changes in $A_{\parallel}$ and $A_{\perp}$ at the identical elapsed times. Thus, F_D can be evaluated in time intervals of 10 s. The drawback of this procedure lies in the fact that the identical sample cannot be used for both of the time-resolved measurements.

II.D. Stress Relaxation Measurements. The stress relaxation at 110 °C, which is the same temperature of the 2d-SAXS measurements, was monitored with TMA 4000 (Mac Science Co., Ltd.) equipped with a 0.5 kg load cell. A film with 3 mm width was squeezed by chucks with a 10 mm interchuck distance. The thickness of the film was ca. 0.1 mm. By quickly placing a stretched sample into a furnace warmed at 110 °C, the time-resolved measurements of the stress relaxation were performed for the stretched sample with $\epsilon = 3.0$.

III. Results

Temporal changes in the 2d-SAXS patterns (through view) upon temperature jump (T-jump) from room temperature to 110 °C under stretched state with $\epsilon = 3.0$ are shown in Figure 3 for the samples cross-linked with $c_X = 0.5$ and 1.5 wt %. The contour lines are drawn every 20% increment in the logarithmic intensity [log $I(q)$], which is normalized 0 to 1 respectively with respect to the minimum and maximum values of log $I(q)$ in the area of Figure 3. Note also that the shaded area in the center of the 2d-SAXS pattern indicates the location of the direct-beam stopper. The stretching direction is vertical, and q denotes the magnitude of the scattering vector, as defined by $q = (4\pi/\lambda) \sin(\theta/2)$ with

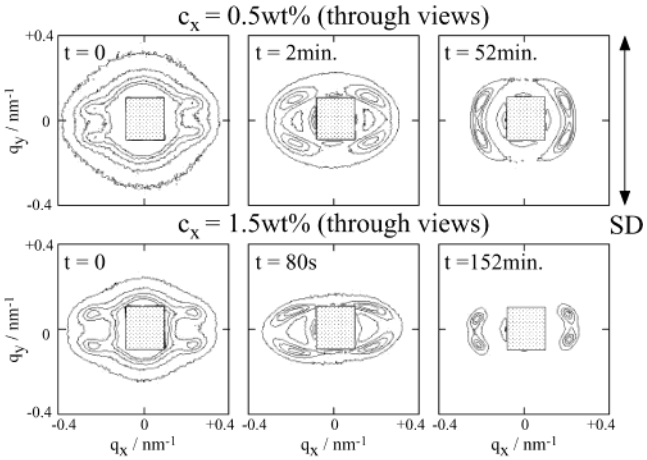

Figure 3. 2d-SAXS patterns (contour plots for the logarithmic intensity for through views) obtained for cross-linked films (c_X = 0.5 and 1.5 wt %) with various annealing time. The films were thermally annealed at 110 °C under stretched state (ϵ = 3). The stretching direction (SD) is vertical.

θ being the scattering angle. The scattering vector q_i is parallel to the i-axis (i: x, y, or z). Although details are different for those two sets of the 2d-SAXS pattern, features of the change are similar. At $t = 0$, i.e., just before the T-jump, four intense spots with streaks parallel to the equator were presented. This kind of pattern is typical of the herringbone structure.[26−28] Upon the T-jump, the four streaks transformed rapidly into oblique streaks, each of which turned into more or less an arc. This tendency was more obvious at each successive stage (at $t = 52$ min for $c_X = 0.5$ wt % and at $t = 152$ min for $c_X = 1.5$ wt %). It seems that a pair of peaks facing each other against the equator merges gradually. Unfortunately, we could not completely follow the long-term process. Instead, the 2d-SAXS pattern (through view) for a final structure is displayed in Figure 4, together with edge and end views of the sample, which was cross-linked with $c_X = 4.0$ wt % and was further annealed at 130 °C for 2 h under stretched state with $\epsilon = 3$. Note here that the sample is not the same as that used for Figure 3. The experimental Cartesian coordinates and measurement geometry corresponding to the through, edge, and end views are schematically shown together in Figure 4a. Note that the y-axis is chosen parallel to the stretching direction (SD) and the z-axis is parallel to the normal of the sample film. Note also that the through view pattern is recorded on the $x-y$ plane by sending the incident X-ray beam from the z-direction. The edge view pattern is recorded on the $y-z$ plane with the incident beam from the x-direction, and the end view pattern appears on the $x-z$ plane with the incident beam from the y-direction. Higher-order diffraction peaks can be identified in the end view pattern. As a matter of fact, the 1d-SAXS profiles, shown in Figure 4b, confirm that the higher-order diffraction peaks are presented up to the third order, where the 1d-SAXS profiles were converted from the 2d patterns by conducting the sector average ($\varphi = 80 \pm 5°$, the definition of φ is shown in the respective 2d-SAXS view with respect to the y-axis (|| SD)) for the edge and through views and by the circular average for the end view. The position of those diffraction peaks can be assigned to 1:2:3, which indicates the lamellar microdomain structure. Judging from all the three views by the analogy of our previous study,[22] one-dimensional and axisymmetric preferential orientation

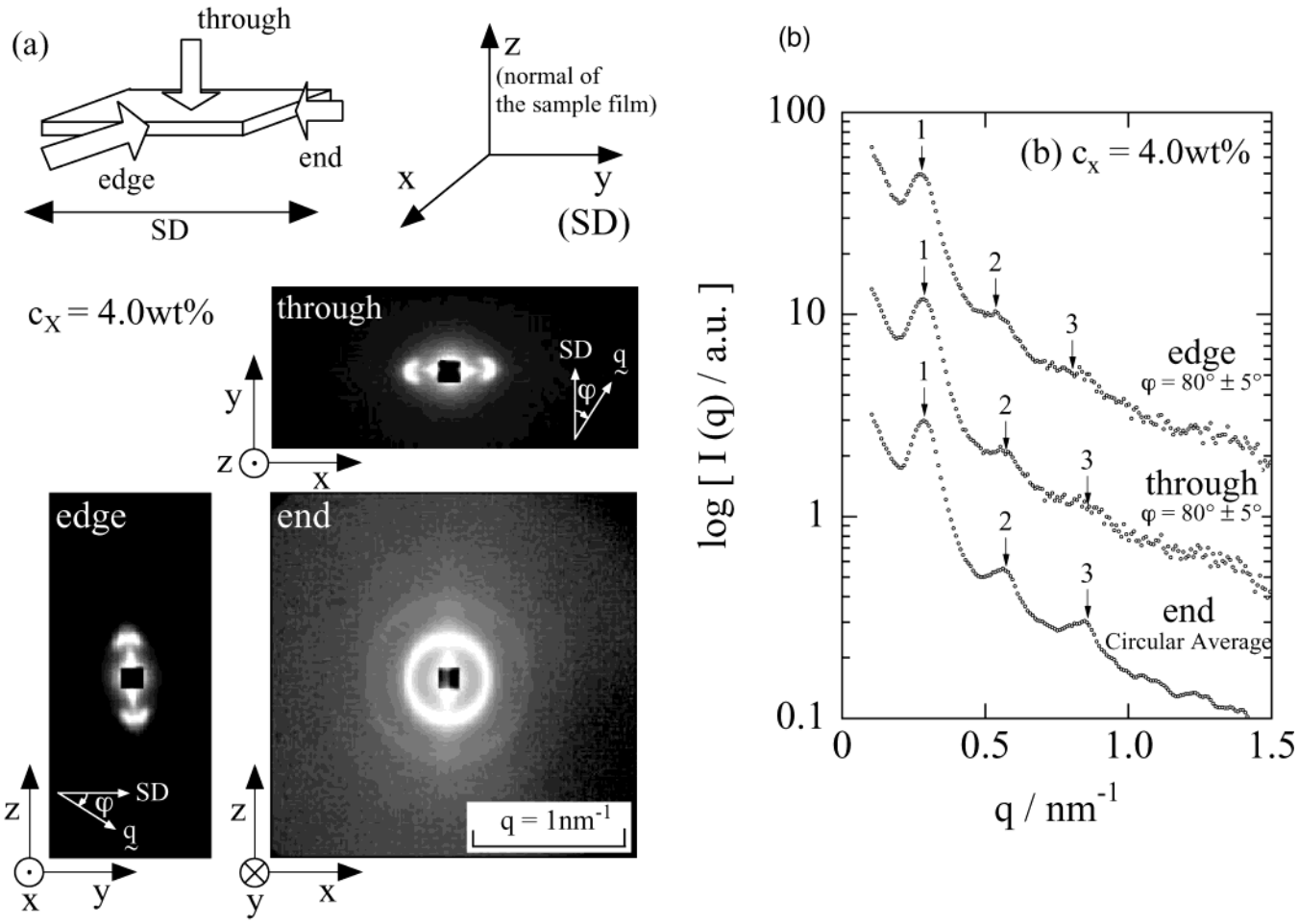

Figure 4. (a) 2d-SAXS patterns (gray scale for the logarithmic intensity) obtained for a cross-linked film (c_X = 4.0 wt %) with annealing at 130 °C for 2 h under stretched state ($\epsilon = 3$). A schematic drawing of the experimental Cartesian coordination and measurement geometry for the through, edge, and end views are shown together. (b) 1d-SAXS profiles (log $I(q)$ vs q) converted from the 2d-SAXS patterns by conducting the sector average over azimuthal angle $\varphi = 80 \pm 5°$ for the through and the edge views and by the circular average for the end view. The φ is defined with respect to the y-axis (|| SD).

of the lamellae can be further concluded as the final structure, which is transformed from the herringbone structure upon the thermal annealing under a stretched state.

On the basis of the results of the change in the 2d-SAXS patterns, a pathway for the structural transformation is considered. First of all, changes in the peak intensity (I_m) are examined. Figure 5 shows the change of I_m with the annealing time, t, where the intensity values at the four peak tops were averaged so as to evaluate I_m. To make a comparison between c_X = 0.5 and 1.5 wt %, the peak intensity is normalized by its initial value at $t = 0$, and the variations of $I_m(t)/I_m(t=0)$ are shown in Figure 5. For both cases, the peak intensity increased abruptly and then saturated. Close examination reveals a two-step increase. For c_X = 0.5 wt %, the increase in the peak intensity was decelerated around t = 1.1 min and completely saturated around t = 4.5 min. As for c_X = 1.5 wt %, this tendency is similar, but the whole process is accelerated by a factor of about 1.15. Namely, the increase in the peak intensity was damped around t = 0.9 min and completely saturated around t = 4.0 min. Subsequently, the peak intensity turned to decrease around t = 10 min. We discuss an origin of the two-step increase of the peak intensity later.

To characterize the herringbone structure, some structural parameters were evaluated from the 2d-SAXS pattern exhibiting the parallel four-streak pattern. A total of five parameters as shown schematically in Figure 6a were chosen to characterize the shape and orientation of the streaklike spots. The shape and peak intensity of each streaklike spot are slightly different among the four due to imperfections in symmetry. Therefore, those parameters evaluated for individual peaks were averaged. Parameters δ and σ denote widths of the peak in the direction perpendicular and parallel

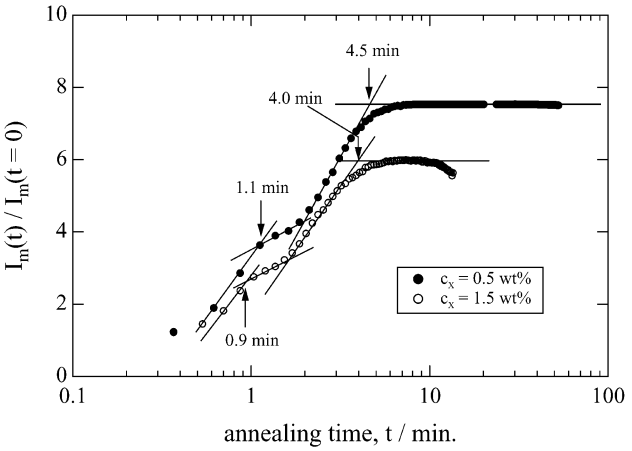

Figure 5. Normalized peak intensity, $I_m(t)/I_m(t=0)$, as a function of the annealing time (t) at 110 °C for cross-linked films (c_X = 0.5 and 1.5 wt %).

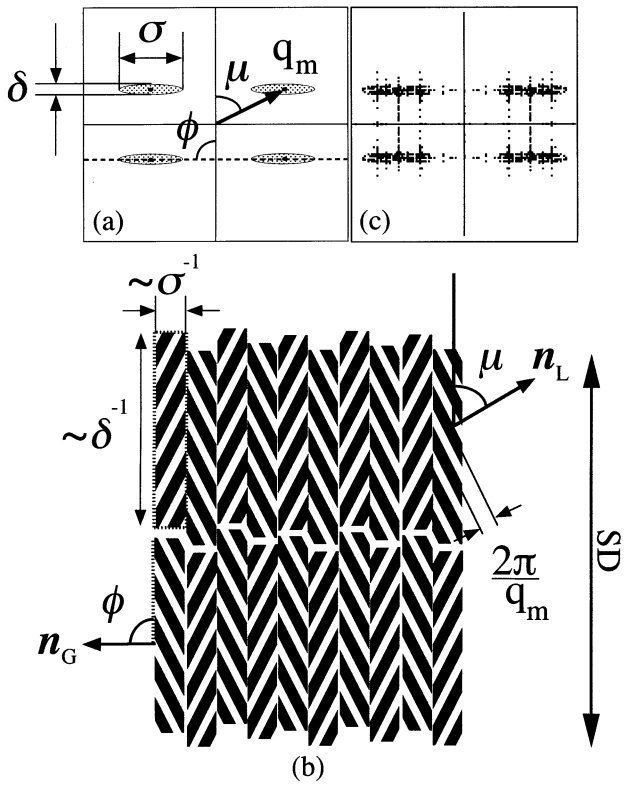

Figure 6. (a) Definitions of parameters characterizing the 2d-SAXS pattern for the herringbone structure. (b) Schematic representation for the herringbone structure. (c) Fast Fourier transformation (FFT) image of the model of the herringbone structure presented in (b).

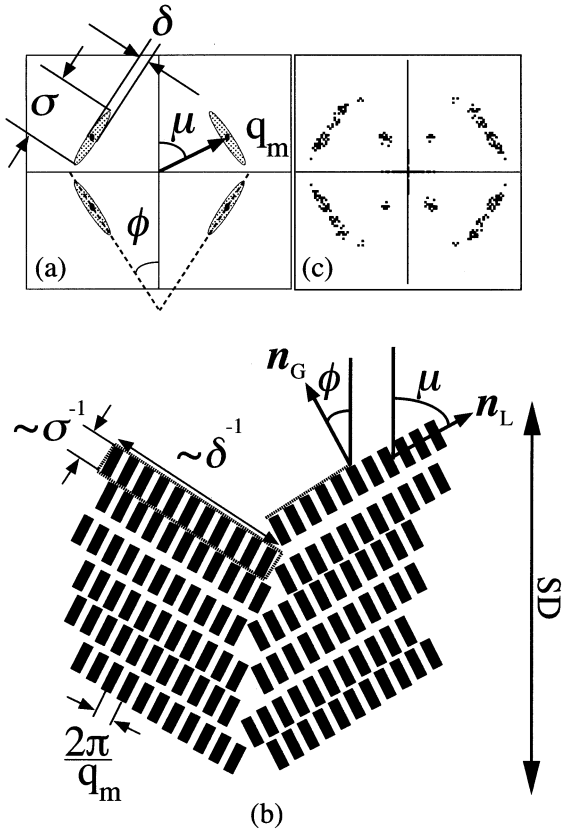

Figure 7. (a) Definition of parameters characterizing the 2d-SAXS pattern for such a model presented in (b). (b) Schematic representation for a transient structure in the course of transformation from the herringbone to the oriented lamella. (c) The FFT image of the structural model presented in (b).

to the main (long) axis, respectively, while ϕ and μ designate respectively an oblique angle of the main axis of a streaklike spot and that of the q vector pointing toward the peak top with respect to the meridian. (The stretching direction of the sample film was parallel to the meridian.) Note also that q_m is the magnitude of the q vector at the peak top. Those five parameters characterize the herringbone structure, which is schematically illustrated in Figure 6b. Here the black-and-white stripe stands for alternating lamellar microdomains that resulted from fracture of lamellae comprising glassy-and-rubbery block copolymers. The herringbone structure is therefore composed of polygrains. According to the results of the transmission electron microscopy, the cross section of the grain was actually observed as a rectangle with a considerably long axis (more likely a whisker).[26,27] The widths δ and σ are inversely proportional to length and width of a rectangular grain. The angles μ and ϕ characterize orientation of the truncated lamellae and obliqueness of the grain with respect to the stretching direction, where n_L and n_G represent the normal vector of the truncated lamellar microdomains and that of the grains, respectively. The repeat period of alternating lamellae is calculated as $2\pi/q_m$. Figure 6c is a resultant FFT (fast Fourier transformation) image of the structural model illustrated in Figure 6b. The characteristic four-streak pattern reproduced confirms the validity of the structural model. To characterize transient structures in the course of transformation from the herringbone to the oriented lamellae, the same structural parameters were evaluated from the 2d-SAXS patterns exhibiting the oblique streak pattern, as is schematically drawn in Figure 7a. The validity of the structural model presented in Figure 7b was also confirmed by the similarity between the FFT image in Figure 7c and the observed 2d-SAXS pattern in Figure 7a.

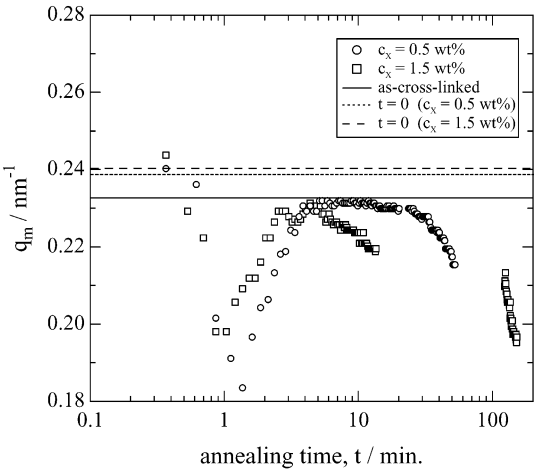

Figure 8. Temporal change in q_m (the magnitude of the q vector at the peak top) for cross-linked films ($c_X = 0.5$ and 1.5 wt %) at 110 °C. The solid, dotted, and broken lines indicate the levels for the as-cross-linked sample and the samples cross-linked with $c_X = 0.5$ and 1.5 wt %, respectively, under stretched state at $\epsilon = 3.0$ before annealing ($t = 0$).

Figures 8−10 show temporal changes in those structural parameters. The value of q_m, shown in Figure 8, decreases rapidly in the initial stage and then increases. It is temporarily saturated at the q_m value for the as-cross-linked sample. The abrupt upturn takes place around $t = 1.3$ and 1.0 min for $c_X = 0.5$ and 1.5 wt %,

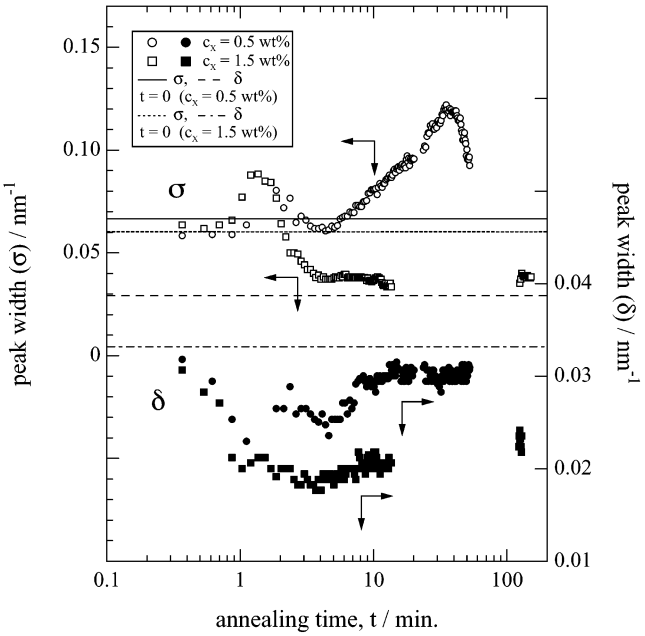

Figure 9. Temporal changes in the peak widths σ and δ. The solid and dotted lines indicate the levels of σ for the samples cross-linked with $c_X = 0.5$ and 1.5 wt %, respectively, under stretched state at $\epsilon = 3.0$ before annealing ($t = 0$), while the broken and dotted-broken lines indicate the levels of δ for the samples cross-linked with $c_X = 0.5$ and 1.5 wt %, respectively, under stretched state at $\epsilon = 3.0$ before annealing ($t = 0$).

respectively, and the saturation of q_m is found around t = 4.5 and 4.0 min, respectively. All such characteristic times are in perfect accord with those for the two-step increase of the peak intensity. These results indicate that the lamellar repeat period first increases rapidly and then decreases gradually. This nonmonotonic behavior can be interpreted, coupled with the change in segmental orientation of PB chains, as discussed below. At very long times, the value of q_m finally starts to decrease for both cases. Temporal changes in the widths δ and σ are shown in Figure 9. The values of σ exhibit nonmonotonic behaviors for both $c_X = 0.5$ and 1.5 wt %, while the value of δ is more or less constant for c_X = 0.5 wt % and monotonically decreases for $c_X = 1.5$ wt %. As for temporal changes in the angles μ and ϕ, shown in Figure 10, a nonmonotonic change is found in μ whereas the values of ϕ exhibit a gradual decrease. However, close examination revealed that the decreasing tendency in ϕ is inflected around $t = 1.5$ min for c_X = 0.5 wt %. As for $c_X = 1.5$ wt %, no change in ϕ is found below $t = 1.0$ min. These characteristic times are in accord with those for the two-step increase in the peak intensity. The final upturn in ϕ is observed above t = 40 min for $c_X = 0.5$ wt %. Roughly speaking, the minimum value of ϕ is 20°, irrespective of c_X. This fact indicates that the orientation of the lamellae parallel to the stretching direction is not completed within the experimental time scale at 110 °C annealing.

IV. Discussion

On the basis of the results of temporal changes in the five structural parameters, the mechanism of the structural transformation from the herringbone structure is considered. To clarify the structural change and to simplify the discussion, it is convenient to highlight the structural change in an individual grain. To characterize the truncated lamellae in the grain, we focus on the

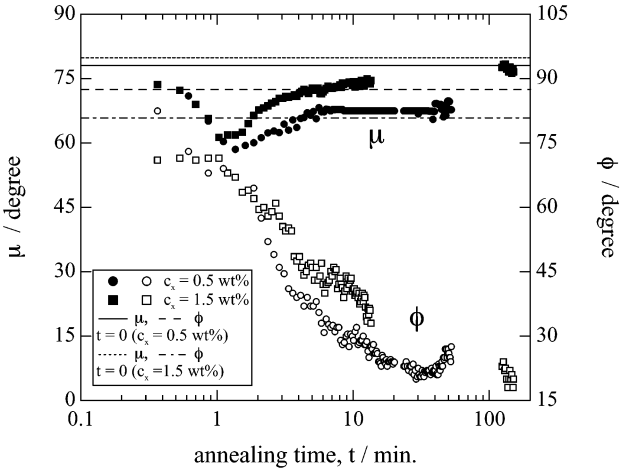

Figure 10. Temporal changes in the angles μ and ϕ. The solid and dotted lines indicate the levels of μ for the samples cross-linked with $c_X = 0.5$ and 1.5 wt %, respectively, under stretched state at $\epsilon = 3.0$ before annealing ($t = 0$), while the broken and dotted-broken lines indicate the levels of ϕ for the samples cross-linked with $c_X = 0.5$ and 1.5 wt %, respectively, under stretched state at $\epsilon = 3.0$ before annealing ($t = 0$).

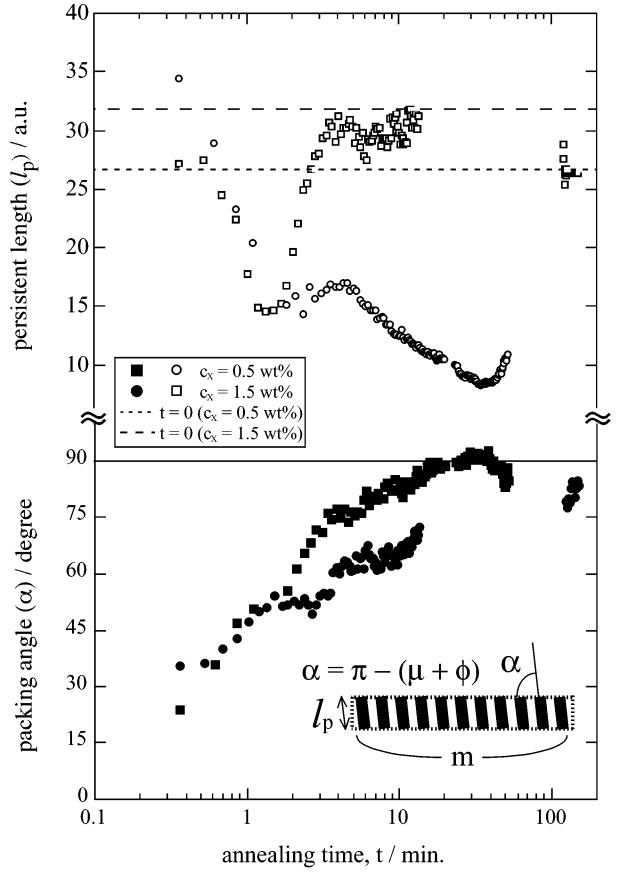

Figure 11. Temporal changes in the persistence length of the truncated lamellae (l_p) and the packing angle (α), where the arbitrary constant k in eqs 1 and 2 was set to unity. The dotted and broken lines indicate the levels of l_p for the samples cross-linked with $c_X = 0.5$ and 1.5 wt %, respectively, under stretched state at $\epsilon = 3.0$ before annealing ($t = 0$). The solid line indicates the level of $\alpha = 90°$.

persistence length of the truncated lamellae (l_p), the packing angle (α), and the number of the lamellae packed in a grain (m), for which definitions are schematically illustrated in Figure 11. Simple geometrical consideration gives the following expressions:

$$l_p = k[\sigma \cos(\mu + \phi - \pi/2)]^{-1}$$
$$\text{for } \alpha \geq \tan^{-1}(\delta/\sigma) \text{ (}k\text{: arbitrary constant)} \quad (1)$$

$$l_p = k[\delta \sin(\mu + \phi - \pi/2)]^{-1} \quad \text{for } \alpha < \tan^{-1}(\delta/\sigma) \quad (2)$$

with

$$\alpha = \pi - (\mu + \phi) \quad (3)$$

and

$$m = kq_m\sqrt{\sigma^{-2} + \delta^{-2}}\cos[\alpha + \tan^{-1}(\delta/\sigma) - \pi/2]$$
$$(k\text{: arbitrary constant}) \quad (4)$$

Thus evaluated values are plotted against the annealing time (t) in Figures 11 and 12, where the arbitrary constant k was set to unity. While the persistence length varies nonmonotonically, the packing angle shows a gradual increase with time, which finally reaches $\alpha =$ ca. 90°, irrespective of c_X. This result indicates that the perpendicular orientation of the truncated lamellae in the grain ($n_L \perp n_G$) is preferred. A similar orientational relationship has been reported by Hashimoto et al. in the initial stage of a formation of a lamellar stack from the disordered (homogeneous) state.[32,33] They considered that the perpendicular orientation minimizes the total free energy of the system. The similarity may suggest that the lamellar orientation in the grain determines the rectangular-like anisotropic shape of the grain. The nonmonotonic variation of l_p is discussed later. The packing number of the lamellae (m) shown in Figure 12 has almost similar tendency for both $c_X = 0.5$ and 1.5 wt %. As a matter of fact, good superposition was obtained in the inset of Figure 12 when the temporal change $m(t)$ was normalized by the initial value of m at $t = 0$. The inconsistency in the very short time range may be due to experimental inaccuracy. The value m increased abruptly for $1.0 < t < 4.5$ min. For $t > 4.5$ min, the value m decreased. The increase is ascribed to the increase in the length (the long axis) of the grain, while the decrease for $t > 4.5$ min can be attributed to not only the decrease in the length of the grain but also the additional effect of an increase of α toward 90° from a value larger than 45°. The illustrations for the structural change are given later in Figures 15 and 16. It is interesting to find that the time for the turnover of m at $t = 4.5$ min coincides with the time at which the segmental orientation of the PB chains was completely relaxed to zero (see Figure 13).

The overall orientation of the truncated lamellae also exhibits nonmonotonic behaviors. As directly shown by the temporal change in μ, the preferential parallel orientation ($\mu \approx 75°$) at $t = 0$ rapidly decreased to $\mu \approx 60°$ but nearly recovered the original value of μ. What governs such a nonmonotonic process of the structural transformation? A clue may lie in the relaxation process of the PB chain orientation. Therefore, we examined the temporal change in the PB chain orientation. The dichroic ratio orientation factor, F_D, for both PS and PB chains is plotted as functions of the annealing time in Figure 13. No appreciable orientation is found for the PS chain because the values of F_D for the PS chain are almost zero within the experimental error. As for the PB chain orientation, F_D shows negative values earlier than $t = 4.0-4.4$ min. Since the direction of the relevant transition moment of the out-of-plane CH bending mode for PB is roughly perpendicular to the main chain, the

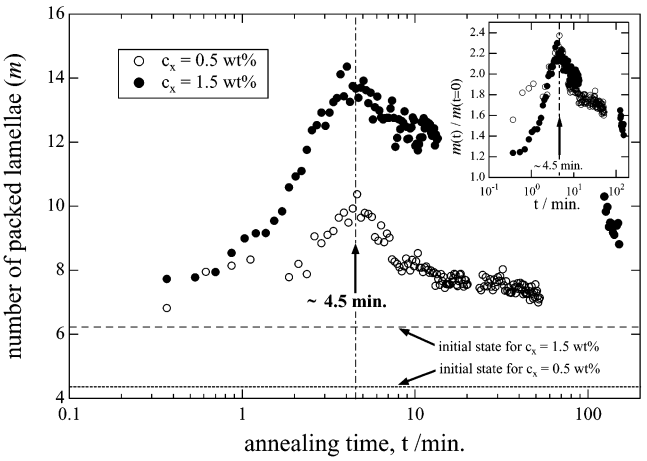

Figure 12. Temporal changes in the number (m) of the truncated lamellae packed in a grain, where the arbitrary constant k in eq 4 was set to unity to evaluate m. The dotted and broken lines indicate the levels of m for the samples cross-linked with $c_X = 0.5$ and 1.5 wt %, respectively, under stretched state at $\epsilon = 3.0$ before annealing ($t = 0$). The normalized plots $m(t)/m(t=0)$ are displayed in the inset.

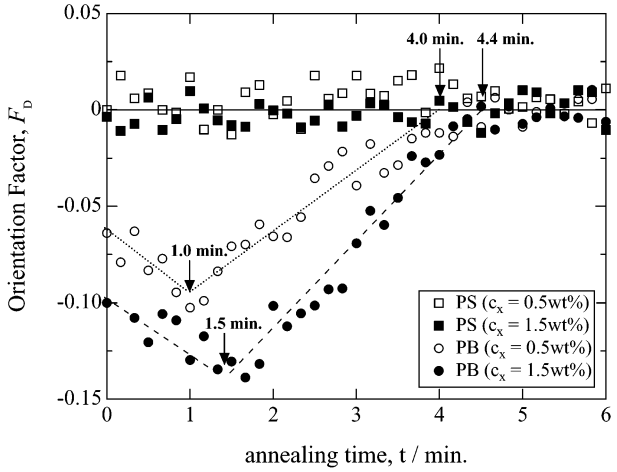

Figure 13. Temporal changes in the dichroic ratio orientation factor, F_D, as functions of the elongation ratio (ϵ) for PS and PB chains.

negative values of F_D indicate the parallel orientation of the PB main chain with respect to the stretching direction. Therefore, the magnitude of the F_D value is a measure of the parallel orientation. The initial orientation of the PB chain is found to be higher for $c_X = 1.5$ wt % due to heavier cross-linking as compared to $c_X = 0.5$ wt %. In the initial stage, earlier than $t = 1.0$ min for $c_X = 0.5$ wt % and earlier than $t = 1.5$ min for $c_X = 1.5$ wt %, further improvement of the parallel orientation is detected. Although the improvement of the parallel orientation of the PB chain is remarkable and rather surprising, the reason is unknown at present. Instantaneously cooperative structural rearrangements involving many grains may give a possible explanation (Figure 15). After the initial stage, the chain orientation undergoes the relaxation toward the unoriented state around $t = 4.0$ min for $c_X = 0.5$ wt % and around $t = 4.4$ min for $c_X = 1.5$ wt %, though the PB chains have been chemically cross-linked. This is simply because the cross-linked polymer networks exist over in the PB microdomains but do not exist in the PS microdomains that can relax the stress by melt flow above $T_{g,PS}$. It is also interesting to find that the structural transformation still continues after the chain relaxation is com-

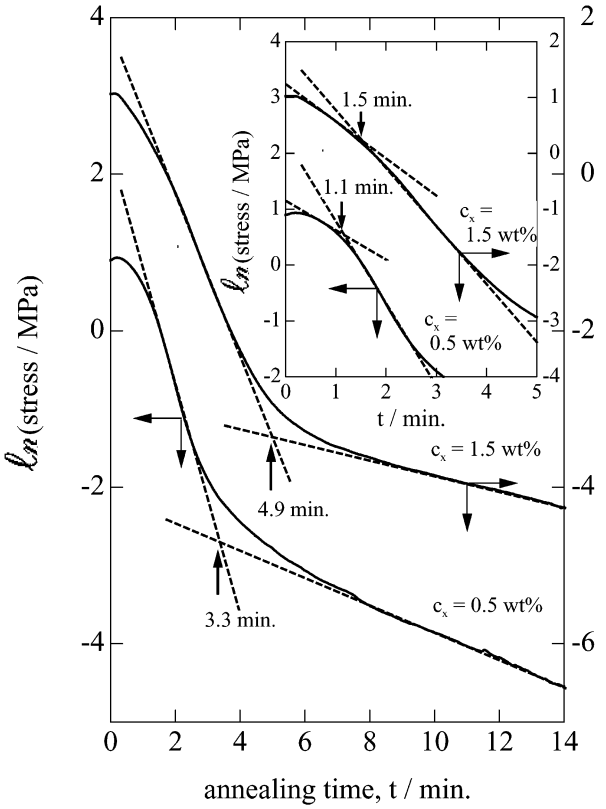

Figure 14. Stress relaxation behaviors at 110 °C for $c_X = 0.5$ and 1.5 wt %. The close-up of the initial stage is presented in the inset.

pleted above those characteristic times. The stress relaxation should correspond to the change in the orientation of the PB chain. As shown in Figure 14, there can be identified three regions that are subdivided with characteristic times that are almost identical to those found in Figure 13. The stress relaxation in the initial stage earlier than $t = 1.1$ min ($c_X = 0.5$ wt %) or $t = 1.5$ min ($c_X = 1.5$ wt %) is less steep as compared to the subsequent stage. This fact suggests that the orientational relaxation of the PB chain would be less remarkable, or it does rather suggest chain orientation as was confirmed by the FTIR measurements (Figure 13). The late stage of the stress relaxation later than $t = 3.3$ min ($c_X = 0.5$ wt %) or $t = 4.9$ min ($c_X = 1.5$ wt %) exhibits a much longer relaxation time. This is considered to be a usual stress relaxation for entangled polymers.

It is suggestive that those characteristic times are in accord with the two-step increase in the peak intensity (Figure 5) and other behavior presented in Figures 8 (q_m), 9 (σ and δ), 10 (μ and ϕ), and 11 (l_p and α). This coincidence may suggest that the orientation of the PB chain governs the process of the structural transformation. In this regard, the mechanism is discussed respectively in regions I, II, and III. The character of each behavior is summarized in Table 1. A shaded part indicates that the behavior is different from each other between $c_X = 0.5$ and 1.5 wt %. Hereafter, the variations in q_m, μ, and l_p are exclusively explained in relation to the conformational changes of the PB chains. Note here that there are common features of variations for both $c_X = 0.5$ and 1.5 wt % in regions I and II. Therefore, we only discuss the case of $c_X = 1.5$ wt %. Figure 15 illustrates the orientational change in the neighboring PS lamellae that are truncated and confined in a grain

Table 1. Comparison of Behaviors in Structural Parameters[a]

$c_X = 0.5$ wt%

Region	I	II	III
Time (min.)	0 ~ 1.3	1.3 ~ 4.5	4.5 ~
I_m (Fig. 5)	+	+	0
q_m (Fig. 8)	− −	+	0 → −
σ (Fig. 9)	0 → + +	−	+ → −
δ (Fig. 9)	−	−	+ → 0
μ (Fig. 10)	−	+	0
ϕ (Fig. 10)	−	−	− → + +
l_p (Fig. 11)	− −	0	− → + +
α (Fig. 11)	+	+	+ → −
magnitude of F_D (Fig. 13)	+	−	0

$c_X = 1.5$ wt%

Region	I	II	III
Time (min.)	0 ~ 1.0	1.0 ~ 4.0	4.0 ~
I_m (Fig. 5)	+	+	0 → −
q_m (Fig. 8)	− −	+	−
σ (Fig. 9)	0 → + +	−	0
δ (Fig. 9)	−	−	+ → 0
μ (Fig. 10)	−	+	0
ϕ (Fig. 10)	0	−	−
l_p (Fig. 11)	− −	+ +	0
α (Fig. 11)	+	+	+
magnitude of F_D (Fig. 13)	+	−	0

[a] Notation: +, increase; + +, steeply increase; −, decrease; − −, steeply decrease; 0, no change (constant).

and the conformational change in the PB chain, which links the neighboring PS lamellae, in the course of the structural transformation for the case of $c_X = 1.5$ wt %. A bunch of grains are shown together to give readers overall structural insights into the corresponding FFT images of the model illustrations. Note that these are quantitatively based on the 2d-SAXS and FTIR results. However, the rectangular shape of the grain is only a simplification, and the number of lamellae packed in the grain is just matched to the value m, which was evaluated by assuming $k = 1$ in eq 4. Furthermore, conversion from the value of F_D to the degree of the PB chain deformation is not straightforward because the quantitative relationship between them is unknown. On the basis of the results reported previously,[30] we can assume that the PB molecular deformation ratio of about 1.4 for $F_D = -0.10$. Note that this value of the F_D was experimentally observed for the case of the most effectively stretching the same SBS sample (TR2400) at the macroscopic deformation of the sample of about 40% elongation. Note also that Cohen et al.[28] reported ca. 1.4 for the maximum value of the deformation ratio in the case of tensile deformation of block copolymers comprising glassy and rubbery lamellae. Therefore, the molecular deformation ratio with respect to the stretching direction was estimated as 1.4, 1.9, 1.1, and 1.0 for $t = 0$, 80 s (region I−II), 4 min (region II−III), and 152 min (region III), respectively. Thus, the model illustrations in Figure 15 were drawn by further assuming the contraction of the chain dimension in the direction perpendicular to the stretching direction by the magnitude compensating for its volume change.

Upon the uniaxial stretching of the original lamellae with the perpendicular orientation (n_L||SD), the herringbone structure results with accompanying the chain stretching of PB. Nevertheless, the interlamellar distance is almost identical to the original one (see Figure 8). According to the illustration presented in Figure 15a, the obliqueness of the truncated lamellae can account for this puzzle. In region I, as shown in Figure 15b, the

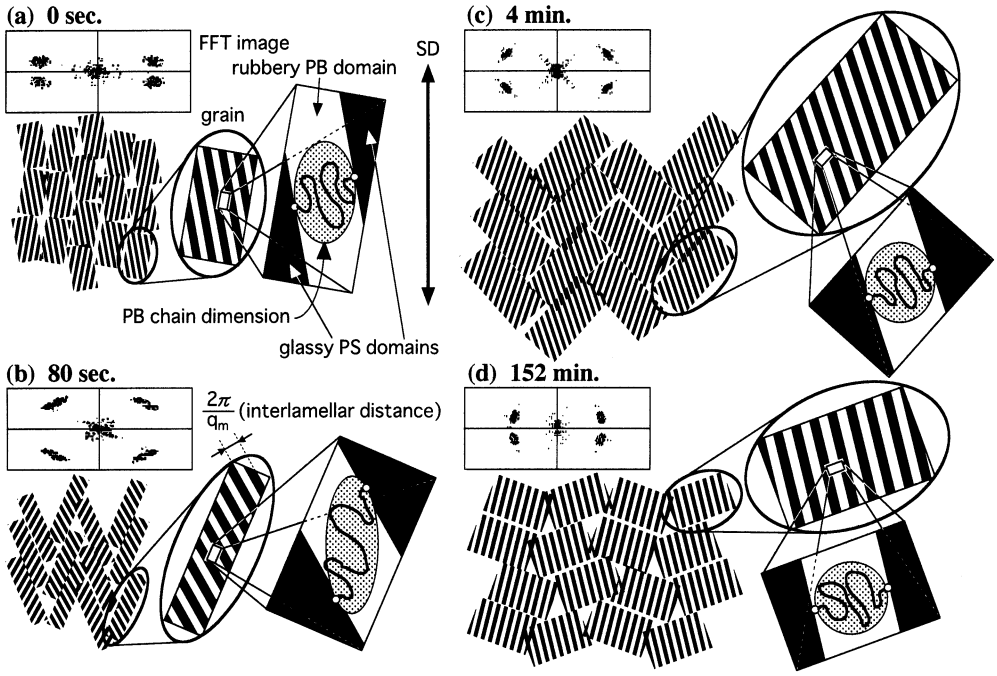

Figure 15. Schematic illustrations showing orientational changes in the neighboring PS lamellae that are truncated and confined in a grain and conformational change in the PB chain that links the neighboring PS lamellae in the course of the structural transformation. A bunch of grains are shown together to give readers overall structural insights into the corresponding FFT images of the model illustrations. Note that these are quantitatively based on the 2d-SAXS and FTIR results.

PB chain is more stretched while the obliqueness is a bit relaxed, both of which contribute increase in the lamellar spacing, namely the decrease in q_m. Note that the relaxation of the lamellar obliqueness is ascribed to the fact that the perpendicular orientation of the truncated lamellae in a grain ($n_L \perp n_G$) is preferred. Because of the relaxation of the lamellar obliqueness within an almost constant width of the grain, l_p decreases and the angle μ also decreases with a slight decrease in ϕ. In region II (Figure 15c), the PB orientation is being relaxed, which causes an increase in q_m, and the obliqueness of the lamellae in the grain continues to relax. In contrast with region I, the width of the grain grows (typically for $c_X = 1.5$ wt %) so that l_p increases. Moreover, the orientation angle μ increases to recover the parallel orientation of lamellae with respect to the stretching direction. Since the PS lamellae are still rigid at 110 °C in the proximity of $T_{g,PS}$, they have a strong tendency to orient parallel to the stretching direction (in the elongational flow). Therefore, the orientation angle μ increases. Meanwhile, the requirement of the perpendicular orientation of the truncated lamellae within the grain should still be met, giving rise to inclination of the grain as shown in Figure 15d and decreasing ϕ toward $\phi = 0°$. In region III, the orientational relaxation of the PB chain is almost complete, and q_m decreases from the value for the original lamellae. Also, the orientation angle μ reaches a constant value. However, the packing angle α is still increasing toward $\alpha = 90°$. Therefore, it can be concluded that region III (the region from Figure 15c to 15d) is governed by the spontaneous perpendicular orientation of truncated lamellae within the grain (not induced by the conformational relaxation of the PB chain), which is now effective to decrease an excess of the free energy by adjusting precisely the orientational mismatch. Since it is required to keep the orientation angle μ unchanged upon the increase in α, this requirement forces the grain to be more inclined and hence decreases ϕ. The packing angle α is still increasing toward $\alpha = 90°$, while the orientational relaxation of the PB chain is almost completed. The relaxation of the obliqueness of the lamellae packed in a grain causes an increase in the lamellar spacing and hence decreases q_m.

Overall, region I is governed by the perpendicular orientation of truncated lamellae within the grain, by which the rapid minimization of the free energy can be attained. On the other hand, region II is governed by the parallel orientation of the PS lamellae in the elongational flow. Again, region III is governed by the perpendicular orientation (spontaneous, not induced by the conformational relaxation of the PB chain) of the truncated lamellae within the grain, which is now effective to decrease an excess of the free energy by adjusting precisely the orientational mismatch.

The illustrations presented in Figure 16 summarize structural changes and finally compare the difference between the cases of $c_X = 0.5$ and 1.5 wt %, by highlighting a single grain. Note that the illustrations were reconstructed by taking account of the temporal changes in the five structural parameters. The stretching direction is vertical. For both cases, the grain first grew long and then turned to become shorter, with continuously inclining (i.e., the value ϕ monotonically decreases). As for the width of the grain, however, continuous thinning is found for $c_X = 0.5$ wt % while temporary thinning followed by a remarkable extent of thickening is identified for $c_X = 1.5$ wt %. Therefore, the grain finally grew bigger in the latter case as compared to the former case. Though the absolute values of the characteristic time were found to differ depending on a run of the 2d-SAXS experiments due to heterogeneity of cross-links and the sample thickness, the reproducibility of the process of the structural change as shown in the two sets of illustrations for $c_X = 0.5$ and 1.5 wt % was confirmed qualitatively.

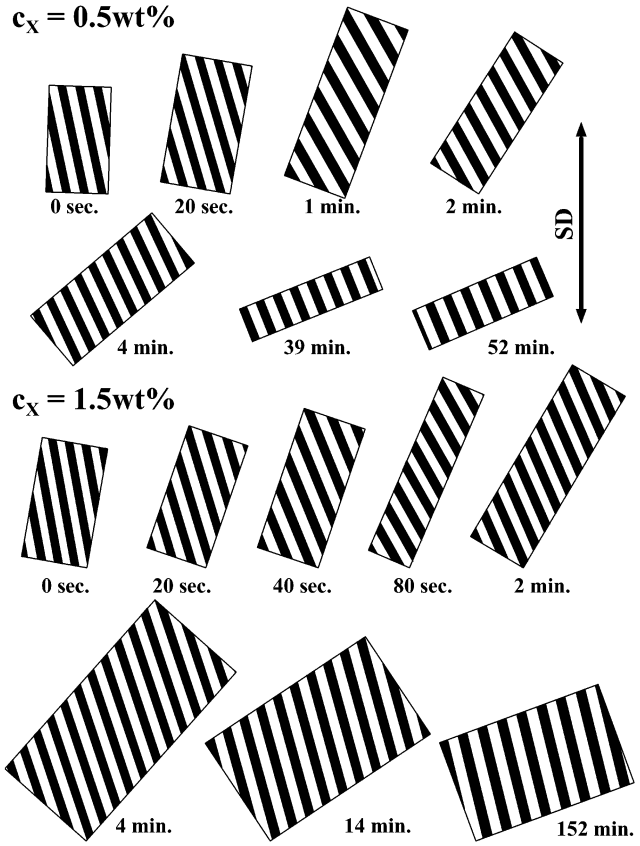

Figure 16. Schematic illustrations highlighting a temporal change of an individual grain. The stretching direction is vertical.

V. Conclusions

The structural transformation from herringbone to preferentially oriented lamellae was analyzed by the time-resolved 2d-SAXS technique. It was found that the process is different depending on the degree of cross-linking. However, each process was found to be divided into three common regions. These regions are governed by the balance between the perpendicular orientation of the truncated lamellae within a grain and the parallel orientation of the PS lamellae with respect to the stretching direction. The conformational changes of the PB chain played a role in controlling the lamellar repeat distance in regions I and II, to which respectively the further chain stretching and the orientational relaxation of the PB chain were relevant.

Acknowledgment. This work is supported in part by the Grant-in-aid from the Japanese Ministry of Education, Culture, Science and Sport (11750781). Synchrotron SAXS experiments were conducted under the approval of the Photon Factory Advisory Committee (Proposal 99G241).

References and Notes

(1) For example, see: Hamley, I. W. *The Physics of Block Copolymers*; Oxford University Press: Oxford, 1998.
(2) Molau, G. E. In Aggarwal, S. L., Ed.; *Block Polymers*; Plenum Press: New York, 1970.
(3) Matsen, M. W.; Bates, F. S. *Macromolecules* **1996**, *29*, 1091.
(4) Khandpur, A. K.; Forster, S.; Bates, F. S.; Hamley, I. W.; Ryan, A. J.; Bras, W.; Almdal, K.; Mortensen, K. *Macromolecules* **1995**, *28*, 8796.
(5) Sakurai, S. *Trends Polym. Sci.* **1995**, *3*, 90.
(6) Leibler, L. *Macromolecules* **1980**, *13*, 1602.
(7) Hashimoto, T.; Tanaka, H.; Hasegawa, H. *Macromolecules* **1985**, *18*, 1864.
(8) Amundson, K.; Helfand, E.; Davis, D. D.; Quan, X.; Patel, S. S. *Macromolecules* **1991**, *24*, 6547.
(9) Scott, D. B.; Waddon, A. J.; Lin, Y. G.; Karasz, F. E.; Winter, H. H. *Macromolecules* **1992**, *25*, 4175.
(10) Serpico, J. M.; Wnek, G. E.; Krause, S.; Smith, T. W.; Luca, D. J.; Laeken, A. V. *Macromolecules* **1992**, *25*, 6373.
(11) Winey, K. I.; Patel, S. S.; Larson, R. G.; Watanabe, H. *Macromolecules* **1993**, *26*, 2542.
(12) Amundson, K.; Helfand, E.; Davis, D. D.; Quan, X.; Smith, S. D. *Macromolecules* **1993**, *26*, 2698.
(13) Almdal, K.; Koppi, K. A.; Bates, F. S. *Macromolecules* **1993**, *26*, 1743.
(14) Morrison, F. A.; Mays, J. W.; Muthukumar, M.; Nakatani, A. I.; Han, C. C. *Macromolecules* **1993**, *26*, 5271.
(15) Okamoto, S.; Saijo, K.; Hashimoto, T. *Macromolecules* **1994**, *27*, 3753.
(16) Okamoto, S.; Saijo, K.; Hashimoto, T. *Macromolecules* **1994**, *27*, 5547.
(17) Amundson, K.; Helfand, E.; Davis, D. D.; Quan, X.; Hudson, S. D.; Smith, S. D. *Macromolecules* **1994**, *22*, 6559.
(18) Jackson, C. L.; Barnes, K. A.; Morrison, F. A.; Mays, J. W.; Nakatani, A. I.; Han, C. C. *Macromolecules* **1995**, *3*, 713.
(19) Panyukov, S.; Rubinstein, M. *Macromolecules* **1996**, *29*, 8220.
(20) Firestone, M. A.; Tiede, D. M.; Seifert, S. *J. Phys. Chem. B* **2000**, *104*, 2433.
(21) Daniel, C.; Hamley, I. W.; Mortensen, K. *Polymer* **2000**, *41*, 9239.
(22) Sakurai, S.; Aida, S.; Okamoto, S.; Ono, T.; Imaizumi, K.; Nomura, S. *Macromolecules* **2001**, *34*, 3672.
(23) Kotaka, T.; Okamoto, M.; Kojima, A.; Kwon, Y. K.; Nojima, S. *Polymer* **2001**, *7*, 3223.
(24) Kota, T.; Sakurai, S.; Aida, S.; Okamoto, S.; Ono, T.; Imaizumi, K.; Nomura, S. *Conf. Proc. ICAPP*, in press.
(25) Aida, S.; Sakurai, S.; Nomura, S. *Polymer*, **2002**, *43*, 2881.
(26) Fujimura, M.; Hashimoto, T.; Kawai, H. *Rubber Chem. Technol.* **1978**, *51*, 215.
(27) Cohen, Y.; Albalak, R. J.; Dair, B. J.; Capel, M. S.; Thomas, E. L. *Macromolecules* **2000**, *33*, 6502.
(28) Cohen, Y.; Brinkmann, M.; Thomas, E. L. *J. Chem. Phys.* **2001**, *114*, 984.
(29) Fujisawa, T.; Inoko, Y.; Yagi, N. *J. Synchrotron Radiat.* **1999**, *6*, 1106.
(30) Sakurai, S.; Sakamoto, J.; Shibayama, M.; Nomura, S. *Macromolecules* **1993**, *26*, 3351.
(31) Sakamoto, J.; Sakurai, S.; Doi, K.; Nomura, S. *Polymer* **1993**, *34*, 4837.
(32) Hashimoto, T.; Sakamoto, N.; Koga, T. *Phys. Rev. E* **1996**, *54*, 5832.
(33) Sakamoto, N.; Hashimoto, T. *Macromolecules* **1998**, *31*, 3815.

MA012259N